

The origin of strong correlations and superconductivity in Na_xCoO_2

Giniyat Khaliullin¹ and Jiří Chaloupka^{1,2}

¹*Max-Planck-Institut für Festkörperforschung, Heisenbergstrasse 1, D-70569 Stuttgart, Germany*

²*Department of Condensed Matter Physics, Faculty of Science, Masaryk University, Kotlářská 2, 61137 Brno, Czech Republic*

(Dated: October 28, 2018)

We propose a minimal model resolving a puzzle of enigmatic correlations observed in sodium-rich Na_xCoO_2 where one expects a simple, free motion of the dilute $S = 1/2$ holes doped into a band insulator NaCoO_2 . The model also predicts singlet superconductivity at experimentally observed compositions. The model is based on a key property of cobalt oxides – the spin-state quasidegeneracy of CoO_6 octahedral complex – leading to an unusual physics of, *e.g.*, LaCoO_3 . We show that correlated hopping between t_{2g} and e_g states leads to the spin-polaron physics at $x \sim 1$, and to an extended *s*-wave pairing at larger doping when coherent fermionic bands are formed.

PACS numbers: 71.27.+a, 74.20.Mn, 74.70.-b

I. INTRODUCTION

Recent studies boosted by the discovery of water-induced superconductivity (SC) in Na_xCoO_2 ¹ exposed many remarkable properties of these compounds² such as a spin-sensitive thermopower³, unusual charge and spin orderings^{4,5,6,7,8}, very narrow quasiparticle bands^{9,10,11,12,13} *etc.* While strongly correlated nature of Na_xCoO_2 is no longer at doubt, the mechanisms by which the correlated electrons design such an exotic phase diagram⁴ are not fully understood even on a qualitative level.

Superconductivity of cobaltates has low $T_c \simeq 5$ K. However, the identification of the pairing mechanism is a problem of principal importance, because this may shed light on the other puzzles of Na_xCoO_2 as well. Moreover, hopeful comparisons with the high- T_c cuprates have been made^{1,14}, noticing that Na_xCoO_2 consists of CoO_2 layers with $S = 1/2$ Co^{4+} ions doped by $S = 0$ Co^{3+} charge carriers, an apparent t_{2g} -band analog of the cuprates. A triangular lattice formed by Co ions, providing favorable conditions for a realization of the resonating-valence-bond (RVB) ideas¹⁵, has been also emphasized.

However, it was quickly realized that: (i) the phase diagram of Na_xCoO_2 ⁴ is radically different from that of cuprates; (ii) SC dome is located at valence compositions closer to $\text{Co}^{3+}(S = 0)$ rather than $\text{Co}^{4+}(S = 1/2)$ (*i.e.*, at average valences $\lesssim 3.50$)^{16,17,18}, not favorable for RVB-theories¹⁹. Further, Na_xCoO_2 shows magnetic order at $x > 0.75$ (besides a particular one at $x = 0.5$ ^{4,7}) which is counter-intuitive because density of Co^{4+} spins $\propto (1 - x)$ decreases at large x . These observations make it clear that the origin and functionality of strong correlations in cobaltates and cuprates are very different.

In this paper, we propose a model for strong correlations that operate over the entire phase diagram of Na_xCoO_2 and lead to SC optimized near the valency 3.4 as observed. First, we consider a single hole doped in NaCoO_2 and show why its behavior is radically different from that of a free carrier embedded in a band insulator. Considering then a Fermi-liquid regime of Na_xCoO_2 , we

demonstrate how an unusual, kinetic energy driven pairing emerges in the model.

The model is based on the following points (none is present in cuprates): (i) typically, Co^{3+} ions in the octahedral environment possess also low-lying magnetic states, *e.g.* $t_{2g}^5 e_g^1 S = 1$ or $t_{2g}^4 e_g^2 S = 2$; (ii) in the CoO_2 planes with 90° Co-O-Co bonds, the correlated $S = 1$ spin states are strongly coupled to the ground state via the intersite $t_{2g} \leftrightarrow e_g$ hopping (see Fig. 1)²⁰. In other words, the magnetic configuration of Co^{3+} ions is activated once the mobile Co^{4+} holes are added in NaCoO_2 . A dynamical generation of $t_{2g}^5 e_g^1 S = 1$ states by a hole motion converts it into a many-body correlated object – the spin-polaron. At larger density of Co^{4+} , we eliminate a virtual $S = 1$ states perturbatively, and find an effective model in a form of spin-selective pair hopping of electrons. The correlated hopping energy is optimized when holes are paired and condense into a SC state.

Spin-state quasidegeneracy of cobalt ions is well known, LaCoO_3 being a textbook example²¹. According to Ref. 22, magnetic states are in the range of $\sim 200 - 400$ meV ($S = 1$) and $\gtrsim 50$ meV ($S = 2$) above the $t_{2g}^6 S = 0$ ground state (without lattice relaxations). A balance between the crystal-field, Hund's coupling and *pd*-covalency is easily tuned and latent magnetism of Co^{3+} living in virtual states can be activated, *e.g.*, by nonmagnetic doping^{23,24}. In oxides with 180° *d-p-d* bonding as in LaCoO_3 , this process leads typically to a ferromagnetic metal stabilized by an electron promoted into broad e_g bands²⁴. New element of Na_xCoO_2 is the 90° *d-p-d* bonding where the e_g - e_g hopping is suppressed. Instead, a large overlap between the neighboring e_g and t_{2g} orbitals is dominant. A curious situation which arises is that while Co^{3+} ions are nonmagnetic in NaCoO_2 , their $S = 1$ $t_{2g}^5 e_g$ configurations are dynamically generated in a doped case by the strong t_{2g} - e_g hopping.

A résumé is that a low-lying magnetic states of Co^{3+} , accessible for electrons via the intersite hopping, provide an extra dimension in physics of Na_xCoO_2 . In Sec. II, we design a model incorporating this idea. Based on this

model, we demonstrate in Sec. III that a hole doped into the band insulator NaCoO_2 behaves in fact as a magnetic polaron dressed by the spin-state fluctuations of Co^{3+} ions that are excited by hole motion. Sec. IV derives the interaction between holes, mediated by virtual spin-state excitations of Co^{3+} ions, in a Fermi-liquid regime at finite hole densities. We also discuss there the relevance of these interactions to the spin ordering, and find signatures of $2k_F$ -instabilities. Finally, we focus in Sec. V on the superconductivity and discuss symmetry and doping dependencies of pairing instabilities within our model. Sec. VI concludes the paper.

II. MODEL HAMILTONIAN

The t_{2g} orbitals in Na_xCoO_2 split into $a_{1g} = (d_{xy} + d_{yz} + d_{zx})/\sqrt{3}$ and $e'_g = (d_{xy} + e^{\pm i\varphi}d_{yz} + e^{\mp i\varphi}d_{zx})/\sqrt{3}$ states ($\varphi = 2\pi/3$). The photoemission experiments^{9,10,11,13} show that a single band, derived mostly from the a_{1g} orbitals, is active near the Fermi level (see Ref. 25 for the orbital-selection mechanism). Therefore, we base our model on the $a_{1g} \equiv f$ hole states (its three-band version will be presented elsewhere²⁶). Valence fluctuations $d_j^6 d_i^5 \rightarrow d_j^5 d_i^6$ within the low-spin t_{2g} manifold read then as $H_t = -t \sum_{ij\sigma} f_{j\sigma}^\dagger f_{i\sigma}$, where $t = 2t_0/3$ and $t_0 = t_\pi t_\sigma / \Delta_{pd}$ is the overlap between t_{2g} orbitals²⁷ (hereafter, a hole representation is used). Our crucial observation is that the t_{2g} - e_g hopping $\tilde{t} = t_\sigma t_\pi / \Delta_{pd}$, which uses a stronger σ -bonding path with $t_\sigma/t_\pi \sim 2$, leads to more effective valence fluctuations. The hopping geometry is depicted in Fig. 1. The nearest neighbor (NN) Co ions and two O ions binding them determine a plane which could be labeled a , b or c according to the Co-Co bond direction. With respect to this plane, the \tilde{t} -hopping couples the in-plane t_{2g} orbital to the out-of-plane e_g orbital.

The \tilde{t} process generates $S = 1$ state of Co^{3+} composed of a t_{2g} hole and an e_g electron; we represent it by \mathcal{T} operator (low-spin $S = 0$ $t_{2g}^5 e_g^1$ state is much higher in energy and can be ignored²⁶). \mathcal{T} is specified by its spin projection and the e_g orbital γ created by \tilde{t} hopping, *i.e.*, $\mathcal{T}_{+1,\gamma}^\dagger = e_{\gamma\uparrow}^\dagger f_{\uparrow}^\dagger$, $\mathcal{T}_{-1,\gamma}^\dagger = e_{\gamma\downarrow}^\dagger f_{\downarrow}^\dagger$ and $\mathcal{T}_{0,\gamma}^\dagger = (e_{\gamma\uparrow}^\dagger f_{\downarrow}^\dagger + e_{\gamma\downarrow}^\dagger f_{\uparrow}^\dagger)/\sqrt{2}$. We are now in position to show our minimal model for Na_xCoO_2 : $H_{t-\tilde{t}} = H_t + H_{\tilde{t}}$, where H_t is as given above, while

$$H_{\tilde{t}} = -\frac{\tilde{t}}{\sqrt{3}} \sum_{ij} \left[\mathcal{T}_{+1,\gamma}^\dagger(i) f_{j\downarrow}^\dagger f_{i\uparrow} - \mathcal{T}_{-1,\gamma}^\dagger(i) f_{j\uparrow}^\dagger f_{i\downarrow} - \mathcal{T}_{0,\gamma}^\dagger(i) \frac{1}{\sqrt{2}} (f_{j\uparrow}^\dagger f_{i\uparrow} - f_{j\downarrow}^\dagger f_{i\downarrow}) + \text{h.c.} \right]. \quad (1)$$

$H_{\tilde{t}}$ moves an electron from Co_j^{3+} to Co_i^{4+} – producing a t_{2g} hole on site j – and replaces the t_{2g} hole on site i by a complex excitation \mathcal{T} . Making use of the t_{2g} - e_g hopping (the *largest* one for 90° Co-O-Co bonds), an electron

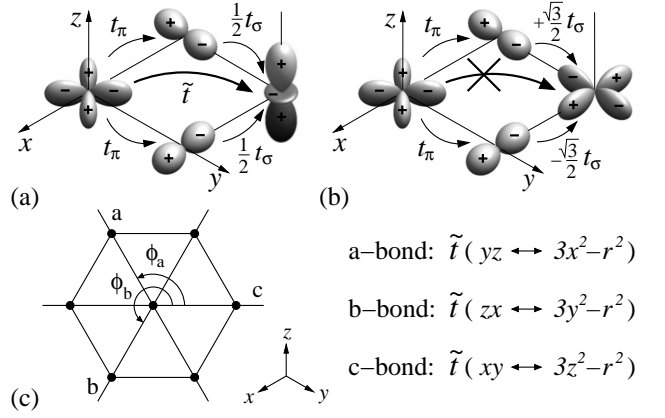


FIG. 1: (a) Electron hopping from t_{2g} to e_g orbital via oxygen atoms in the case of 90° bonds creating $S = 1$ $t_{2g}^5 e_g$ configuration of Co^{3+} . The t_{2g} orbital laying in the plane (here the xy orbital) couples to the out-of plane e_g ($3z^2 - r^2$) orbital. (b) The coupling to the planar orbital is zero because of the destructive interference of two channels. (c) Bond directions and corresponding angles in the hexagonal lattice of Co ions and \tilde{t} -active orbitals on these bonds.

“picks-up” the spin correlations in virtual states. The index γ is determined by the orientation of the $\langle ij \rangle$ bond according to the rules in Fig. 1(c). The overlap between e_g orbitals specified by γ and γ' is $\langle \gamma | \gamma' \rangle = \cos(\phi_\gamma - \phi_{\gamma'})$. Consequently, the excitations \mathcal{T}_γ inherit the same overlap: $\langle \mathcal{T}_\gamma \mathcal{T}_{\gamma'} \rangle \propto \langle \gamma | \gamma' \rangle$. The \mathcal{T} -excitation energy E_T is determined by all the many-body interactions within the CoO_6 complex (Hund’s coupling, $p - d$ covalency, crystal field, ...) ²². This is a free parameter of the model. Experimentally, $S = 1$ states of CoO_6 complex in perovskite compound LaCoO_3 are found at energies $E_T \sim 0.2 - 0.4 \text{ eV}$ ²² as already mentioned in the introduction. Based on this observation, we will use in this paper a representative value $E_T \simeq 0.3 \text{ eV}$ for layered cobaltates. In units of a_{1g} hopping integral $t \simeq 0.1 \text{ eV}$ (which follows from the band structure fit $t_0 \simeq 0.15 \text{ eV}$ ²⁵), this translates into $E_T/t = 3$ adopted below in our numerical data. (In principle, we expect some material dependence of E_T as it is decided by the balance of several competing interactions. It is therefore highly desirable to quantify a multiplet structure of CoO_6 -complex in Na_xCoO_2 as done in LaCoO_3 ²²). For the ratio of the hopping amplitudes \tilde{t} and t_0 , we set $\tilde{t}/t_0 = 2$ as $t_\sigma/t_\pi \sim 2$.

III. SPIN-STATE POLARON

It is instructive to consider first a single hole doped in NaCoO_2 . With H_t alone, it is just a usual plane-wave having nothing common with what is actually seen in Na_xCoO_2 at large x . Things change radically when the $H_{\tilde{t}}$ is switched on: now, a hole generates a multiple of \mathcal{T} excitations [see Fig. 2(b)], and spin-polaron physics of

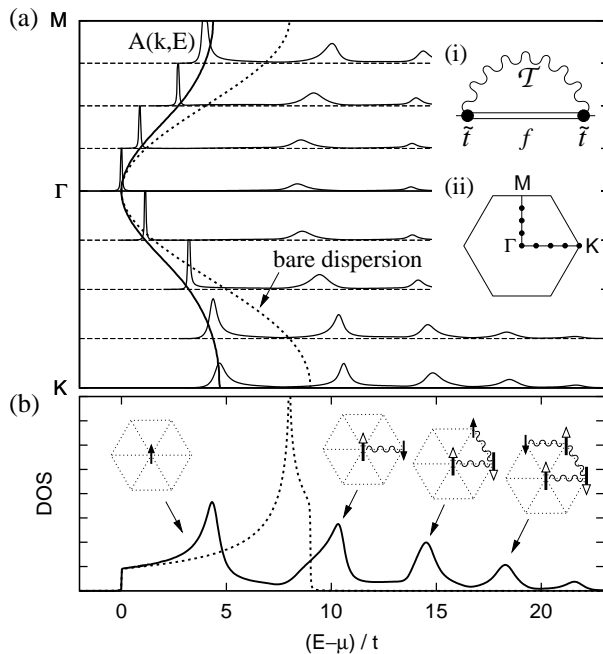


FIG. 2: (a) Spectral functions of a Co^{4+} hole doped in NaCoO_2 along M- Γ -K path in the Brillouin zone [inset (ii)]. Bare and renormalized dispersions, measured both from the chemical potential for better comparison, are shown. (The polaron binding-energy shift is $E_b \simeq 2.6t$). (i) The diagram describing the dressing of a hole by $S = 1$ \mathcal{T} -excitations. (b) Density of states compared to that of the bare band. Virtual processes associated with the polaronic spectral features are sketched: every use of \tilde{t} hopping channel generates $S = 1$ states of Co^{3+} behind the hole.

a typical Mott insulator emerges. Given that NaCoO_2 itself is nonmagnetic at all²⁸, the correlated behavior of doped holes in layered cobaltates has been a mystery; it is resolved here by invoking a “virtual Mottness” of cobalt oxides²⁹ hidden in their low-lying magnetic states.

Polaron physics is evident from the spectral functions in Fig. 2. We have employed a self-consistent Born approximation for the selfenergy, which then takes the form:

$$\Sigma(\omega) = 2\tilde{t}^2 \sum_{\mathbf{k}} \frac{\Gamma_{\mathbf{k}}}{\omega - E_T - \xi_{\mathbf{k}} - \Sigma(\omega - E_T) + i\delta}. \quad (2)$$

Here, $\Gamma_{\mathbf{k}} = c_a^2 + c_b^2 + c_c^2 - c_a c_b - c_b c_c - c_c c_a$ is a geometrical factor coming from the e_g orbital overlap, $\xi_{\mathbf{k}} = -2t(c_a + c_b + c_c) + \mu$ is the bare dispersion in hole representation, and $c_\alpha = \cos k_\alpha$ with k_α are projections of \mathbf{k} on a, b, c axes in the 2D hexagonal lattice of Co ions [Fig. 1(c)]. As the \mathcal{T} -exciton has no dispersion (e_g - e_g hopping is zero in 90° -case), the selfenergy is momentum independent. Strong renormalization of the quasiparticle band and appearance of the incoherent sidebands as seen in Fig. 2 are the characteristic features of polaron formation. Excitations relevant here are the *spin-state* fluctuations of Co^{3+} ions, and a fermionic hole dressed by these excitations can be termed as *spin-state*

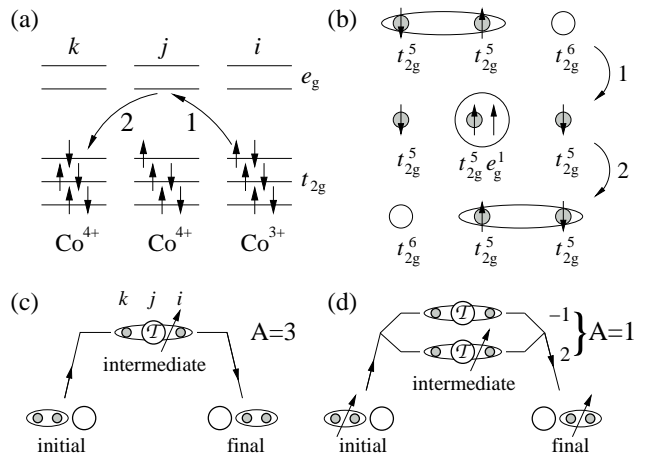


FIG. 3: (a) The physical picture behind Eq. (3). t_{2g} electron of a Co^{3+} ion moves to e_g level of the NN Co^{4+} ion (process 1) and then to the t_{2g} level of the next Co^{4+} neighbor (process 2). This is depicted in (b) as a motion of the hole-pair. (c) Singlet-pair motion via an intermediate state composed of $S = 1$ Co^{3+} ion (\mathcal{T} -exciton) and triplet state of the two holes on $\langle ik \rangle$ -bond. The relative amplitude A resulting from spin algebra is indicated. (d) The triplet-pair hopping amplitude A is three times smaller because of the destructive interference of contributions involving singlet and triplet $\langle ik \rangle$ -bond.

polaron. Physically, it is different from a typical magnetic polaron formed in Mott insulators with a magnetically active ground state, while NaCoO_2 is a nonmagnetic band insulator.

At large $x \sim 1$ limit, dilute polarons are readily trapped by a random potential of Na-vacancies^{30,31}. When the binding is strong, physics is local and a polaron takes a form of hexagon-shaped $S = 1/2$ object where a hole is oscillating to optimize both t and \tilde{t} channels. Our model provides a microscopic basis for spin-polarons introduced on experimental grounds^{5,8,13} and discussed in detail in Refs. 29,32. When the density of polarons is increased (as x decreases), they start to overlap forming narrow bands. Eventually, the polaron picture breaks down and a correlated Fermi-liquid emerges when x is further reduced.

IV. EFFECTIVE INTERACTION BETWEEN t_{2g} HOLES

In the Fermi liquid regime, the Eliashberg-formalism, where the phonon shake-up processes (triggered by \mathcal{T} -exciton) can also be incorporated, would be the best strategy. However, there are delicate constraints to handle: a lattice site cannot be occupied by two holes or by a hole and \mathcal{T} -exciton simultaneously. For the sake of simplicity, we derive an effective fermionic interaction in a second order perturbation theory in \tilde{t} by considering the local virtual process depicted in Fig. 3(a,b).

This way, all the constraints in the intermediate states are treated explicitly. Such a perturbative treatment is valid as long as a polaron binding energy E_b (an energy gain due to the \tilde{t} process) is small compared to a bare bandwidth W ($\simeq 9t$ in a triangular lattice). From a self-consistent Born approximation discussed above, we obtained $E_b \simeq 2.6t \sim 0.3W$ for $\tilde{t} = E_T = 3t$ used in this paper. For this set of parameters, we can therefore integrate out a virtual spin states perturbatively.

As a result, we arrive at the following effective Hamiltonian in two equivalent forms:

$$H_{\text{eff}} = \frac{1}{2}V \sum_{\langle ijk \rangle} \cos(\phi_{ij} - \phi_{jk}) \left[\hat{S}_{ij}^\dagger \hat{S}_{kj} + \frac{1}{3} \hat{T}_{ij}^\dagger \hat{T}_{kj} \right] \quad (3)$$

$$= V \sum_{\langle ijk \rangle} \cos(\phi_{ij} - \phi_{jk}) \left[n_j n_{ik} - \frac{1}{3} \mathbf{s}_j \cdot \mathbf{s}_{ik} \right]. \quad (4)$$

We introduced here a constant $V = \tilde{t}^2/E_T$. Sites $i \neq k$ are the nearest neighbors of site j . The angles $\phi \in (2\pi/3, 4\pi/3, 0)$ are selected by the orientation of the bonds $\langle ij \rangle$ and $\langle jk \rangle$ as already explained. No-double-occupancy constraint on f is implied when using this effective Hamiltonian. The Hamiltonian in Eq. (3) describes the motion of the spin-singlet $\hat{S}_{ij} = (f_{i\uparrow} f_{j\downarrow} - f_{i\downarrow} f_{j\uparrow})/\sqrt{2}$ and spin-triplet $\hat{T}_{ij} = \{f_{i\uparrow} f_{j\uparrow}, \dots\}$ $\text{Co}^{4+}\text{-Co}^{4+}$ pairs in a background of $S = 0$ Co^{3+} ions, and may lead to the pairing instability as shown below.

Alternatively, Eq. (4) represents the same interaction in a form of density-density and spin-spin correlations, emphasizing its relevance also to the charge and spin orderings. Note that n_{ik} and \mathbf{s}_{ik} with $i \neq k$ are the charge and spin densities residing on bonds, *i.e.*, $n_{ik} = \frac{1}{2} \sum_{\sigma} f_{i\sigma}^\dagger f_{k\sigma}$, $\mathbf{s}_{ik}^z = \frac{1}{2} \sum_{\sigma} \sigma f_{i\sigma}^\dagger f_{k\sigma}$ (while $n_j = n_{jj}$ and $\mathbf{s}_j = \mathbf{s}_{jj}$ are the usual on-site operators), so that the interaction acts between the local (*on-site*) and non-local (*bond*) operators. In a momentum space, Eq. (4) can be written as

$$H_{\text{eff}} = 2V \sum_{\mathbf{q}} \left[n_{-\mathbf{q}} \tilde{n}_{\mathbf{q}} - \frac{1}{3} \mathbf{s}_{-\mathbf{q}} \cdot \tilde{\mathbf{s}}_{\mathbf{q}} \right], \quad (5)$$

with the operators $\tilde{n}_{\mathbf{q}} = \frac{1}{2} \sum_{\mathbf{k}, \sigma} F_{\mathbf{k}+\mathbf{q}, \mathbf{k}} f_{\mathbf{k}+\mathbf{q}, \sigma}^\dagger f_{\mathbf{k}, \sigma}$, $\tilde{\mathbf{s}}_{\mathbf{q}}^z = \frac{1}{2} \sum_{\mathbf{k}, \sigma} \sigma F_{\mathbf{k}+\mathbf{q}, \mathbf{k}} f_{\mathbf{k}+\mathbf{q}, \sigma}^\dagger f_{\mathbf{k}, \sigma}$, *etc.* The formfactor $F_{\mathbf{k}', \mathbf{k}} = \cos(k_a + k'_a) + \cos(k_b + k'_b) + \cos(k_c + k'_c) - c_a c'_b - c_b c'_a - c_b c'_c - c_c c'_b - c_c c'_a - c_a c'_c$, where $c'_\alpha = \cos k'_\alpha$, originates from a peculiar bond-dependence of interactions in Eq. (4). It manifests again that the $\tilde{n}_{\mathbf{q}}$ and $\tilde{\mathbf{s}}_{\mathbf{q}}$ operators correspond to the particle-hole excitations that modulate the charge and spin bonds, respectively.

To illustrate this unusual, nonlocal nature of correlations we show in Fig. 4 the effect of the interaction on the spin susceptibility within the RPA approximation. The bare spin susceptibility [Fig. 4(b)] is concentrated around the Γ point. When the interaction is switched on [Fig. 4(c)], the $2k_F$ ring in the susceptibility is enhanced. This suggests the fermionic $2k_F$ -instabilities in a *Fermi-liquid* phase, consistent with a picture inferred from the

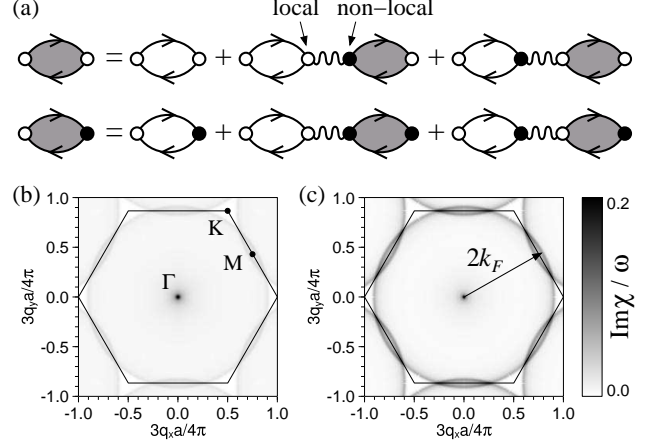


FIG. 4: (a) Diagrammatic representation of RPA equations for the spin susceptibilities involving the interaction Eq. (5) between $\mathbf{s}_{\mathbf{q}}$ (local) and $\tilde{\mathbf{s}}_{\mathbf{q}}$ (non-local) spin densities that reside on sites and bonds, respectively. Bare and RPA-enhanced susceptibilities are represented by empty and shaded bubbles respectively. (b) Map of bare χ''_s/ω for $n_d = 0.5$ (the average Co-valency 3.5) at $T = 0.025t$ and $\omega = 0.005t$. (c) Corresponding RPA-enhanced susceptibility calculated at $\tilde{t}^2/E_T = 3t$. The interaction enhances the susceptibility at the $2k_F$ ring which (at given density $n_d = 0.5$) nearly matches the Brillouin zone boundary.

experiment³³. Interestingly, the RPA-spin susceptibility at $n_d = 0.5$ is most enhanced near the M point, *i.e.* near the observed magnetic Bragg peak position⁷, rather than at K typical for the AF Heisenberg spin system. In order to study the spin ordering at $n_d = 0.5$ more quantitatively, one should take into account also the Na ordering⁴ which breaks a hexagonal symmetry of the underlying Fermi-surface.

V. SUPERCONDUCTIVITY DUE TO THE PAIR-HOPPING INTERACTION

Now, we consider the above Hamiltonian in the context of superconductivity. It is evident from Eq. (3) that spin-singlet pairs gain much more kinetic energy than triplets. As explained in Fig. 3, this nontrivial result originates from a quantum interference between different realizations of the virtual \tilde{t} process. The $S = 1$ \mathcal{T} -excitation in the intermediate state is fully transparent for singlets which equally use all three $S_z = \pm 1, 0$ states of \mathcal{T} . However, in the case of triplet pairs, there exist two quantum paths contributing with opposite signs, which results in a “spin blockade” for the motion of triplets. Alternatively, it can be said that the $S = 0$ Co^{3+} states move more coherently when the $S = 1/2$ background is in a singlet state. The difference from cuprates is that singlets are formed here not due to the superexchange (in cobaltates, J is small¹⁹) but because of the gain in the kinetic energy associated with \tilde{t} hoppings.

A mean-field BCS analysis of Eq. (3) shows that H_{eff} supports either extended s -wave singlet SC with the gap function $\propto \gamma(\mathbf{k}) = \sqrt{2/3}(c_a + c_b + c_c)$, or doubly-degenerate spin-triplet p -wave pairing with $\gamma_{x,y}(\mathbf{k}) = \{(s_a - s_b), (2s_c - s_a - s_b)/\sqrt{3}\}$, where $s_\alpha = \sin k_\alpha$. The d -wave channel is repulsive, while f -wave one is attractive but too weak in the physically reasonable doping range. We estimated the T_c from

$$1 = \sum_{|\bar{\xi}_{\mathbf{k}}| \leq E_T} \frac{\bar{V}_\alpha |\gamma_\alpha(\mathbf{k})|^2}{2\xi_{\mathbf{k}}} \tanh \frac{\bar{\xi}_{\mathbf{k}}}{2T_c}, \quad (6)$$

where \bar{V}_α is either \bar{V} or $\bar{V}/3$, and the corresponding form-factors are $\gamma(\mathbf{k})$ or $\gamma_{x,y}(\mathbf{k})$ for the singlet s -wave and triplet p -wave pairing, respectively. To account for the no-double-occupancy constraint, the fermionic dispersion as well as the pair-hopping amplitude are renormalized by the Gutzwiller factor²⁵ $g_t = 2n_d/(1 + n_d)$ as $(\bar{\xi}, \bar{V}) = (g_t \xi, g_t V)$, where n_d is the relative fraction of Co^{3+} ions. (The reported Co-valences ~ 3.4 ¹⁶, ~ 3.3 ¹⁷, ~ 3.46 ¹⁸ optimal for SC translate then to $n_d = 0.6, 0.7, 0.54$). In the momentum summation, we have introduced a cutoff equal to the excitation energy E_T .

We solved Eq. (6) at $V = 3t$ (as it follows from $\tilde{t} = E_T = 3t$ used in previous sections). In terms of the BCS-coupling constant, this translates into $\lambda = \bar{V}\bar{N} = VN \sim 1/3$ considering the density of states $N \sim 1/W \sim 1/9t$. Therefore, the present formulation in terms of an effective fermionic Hamiltonian (3) should give a reasonable results. At larger values of V , we encounter a strong coupling regime where one should use instead the original model (1) and treat a virtual spin states explicitly. This limit remains a challenging problem for future study.

The resulting T_c values from Eq. (6) are presented in Fig. 5(a) as solid lines. As expected, the highest T_c values are found in the singlet channel, increasing with Co^{3+} density due to the formfactor effect, until SC disappears at $n_d = 1$ limit. A weak triplet pairing is present thanks to its formfactor matching well the Fermi surface, but it is expected to be destroyed by (*e.g.* Na) disorder. (We should notice that these trends are based on the present mean-field decoupling which ignores a collective spin fluctuations. One can speculate, for instance, that the triplet pairing may be supported by a ferromagnetic fluctuations within the CoO_2 planes observed⁶ at large n_d limit).

As the SC pairing considered here is due to the pair-hopping, Coulomb repulsion between the holes will oppose it. This is not a big trouble at high density of Co^{4+} spins (as they cannot avoid themselves) but becomes a severe issue in a spin-diluted regime at large n_d , where Coulomb repulsion reduces the process described in Fig. 3 hence the amplitude V . Instead, the formation of spatially separated spin-polarons (Fig. 2) is favored, and competing orderings take over, such as an in-plane ferromagnetism induced by a residual interactions between spin-polarons³². To include the effects related to the Coulomb repulsion in the Gutzwiller fashion, we

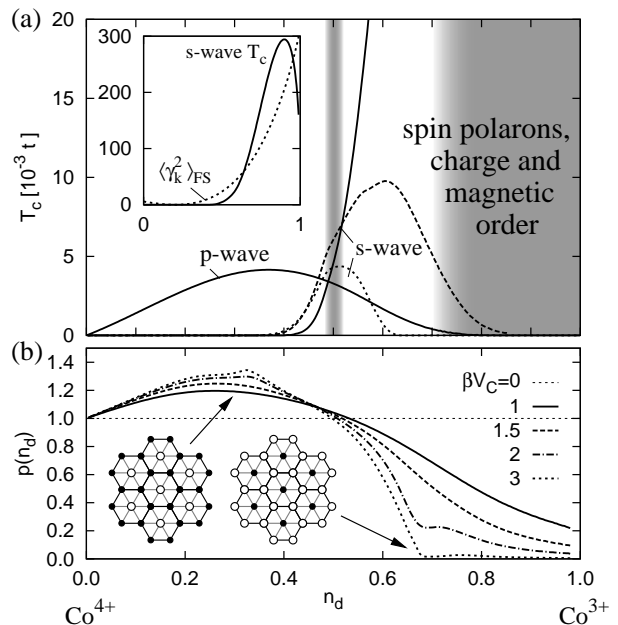


FIG. 5: (a) T_c in the extended s -wave and p -wave channels. The complete profile of the dominant, s -wave T_c curve is shown in the left inset together with $\gamma_{\mathbf{k}}^2$ (in arbitrary units) on the Fermi surface. The dashed ($\beta V_C = 1.5$) and dotted ($\beta V_C = 3$) T_c curves are calculated including NN Coulomb repulsion which reduces the pairing interaction V at large n_d . Shaded regions indicate the observed competing orderings (including the spin-charge order at $n_d = 0.5$). (b) Probability ratio $p(n_d)$ (see text for definition) renormalizing the pairing interaction at different values of NN Coulomb repulsion relative to the effective temperature $1/\beta \propto$ bandwidth. The feature at $n_d = 1/3$ for large V_C manifests a honeycomb-lattice formation where each Co^{3+} (o) has the maximum possible number of neighboring Co^{4+} - Co^{4+} pairs (●-●). Above $n_d = 2/3$, Co^{4+} holes can avoid each-other completely if V_C is sufficiently large.

use an additional multiplicative factor reflecting the suppression of the probability P_{ijk} of having the required $\text{Co}_i^{3+}-\text{Co}_j^{4+}-\text{Co}_k^{4+}$ configuration. We have determined this probability using a classical Monte-Carlo simulation of hardcore particles with NN Coulomb repulsion V_C . The simulations were performed at different “effective temperatures” $1/\beta$ imitating the kinetic energy (of the order of bandwidth) which competes with the Coulomb repulsion in the real system. Plotted in Fig. 5(b) is the probability ratio $p(n_d) = P_{ijk}(V_C)/P_{ijk}(V_C = 0)$ for several values of βV_C . The corresponding T_c curves calculated with $\bar{V} \rightarrow p(n_d)\bar{V}$ locate the SC-dome near the valence 3.4, in a remarkable correspondence with experiment^{16,17,18}.

Finally, our $t - \tilde{t}$ model provides a clear hint on the role of water-intercalation needed for SC in Na_xCoO_2 . Without water, a random Na-potential induces some amount of spin-polarons locally (the origin of “Curie-Weiss metal”⁴) which suppress the pairing among the

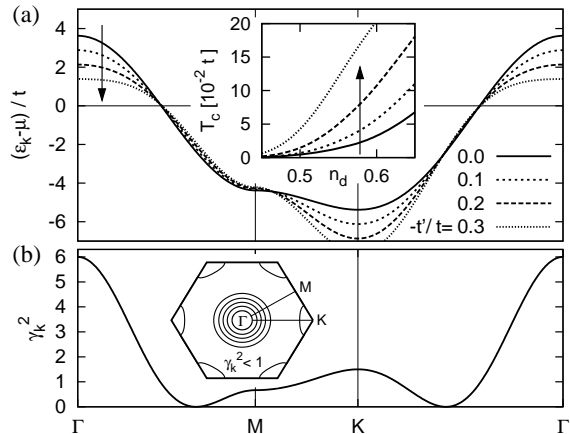


FIG. 6: (a) Band structure for different values of t'/t ($n_d = 0.6$) and the corresponding effect on the s -wave transition temperature. As the band dispersion near Γ point comes closer to the Fermi level, it can exploit the larger formfactor and T_c increases as shown in the inset. The increase is also partially induced by the decreased Fermi velocity along Γ -M direction. (b) Formfactor of the extended s -wave pairing interaction. The inset shows the contours for $\gamma_{\mathbf{k}}^2 = 1, 2, 3, 4, 5$.

remaining fermions the usual way. Once this potential is screened-out by the water layers, an intrinsic ground state of CoO_2 planes as in Fig. 5 is revealed. (This interpretation of the water effect is consistent with the absence of superconductivity in the monolayer hydrate of Na_xCoO_2 , where the water resides in the Na layers.) The remaining “enemy” of SC is the Coulomb repulsion which prevents the pairing of dilute Co^{4+} fermions and supports the formation of spin-polarons and magnetism instead. More pronounced polaron physics (because of the presence of large $S = 1$ \mathcal{T} -exciton and narrow bandwidth) explains why T_c in cobaltates is low compared to cuprates.

Another mechanism for the water effect is provided by the band-structure calculations³⁴ that indicate a substantial flattening of the a_{1g} band-top and a reduction of the band splitting when the water-layers are present.

To study the former effect, we include negative t' in our calculation. Due to the combined effect of better formfactor utilization in s -wave channel and Fermi velocity reduction this enhances singlet pairing as presented in Fig. 6. In triplet channel, on the other hand, the t' -effect is weaker as it includes only the latter factor, *i.e.*, the enhancement due to the reduced Fermi velocity (p -wave formfactor utilization is not very sensitive to t').

VI. CONCLUSIONS

To summarize, we have presented $t - \tilde{t}$ model for Na_xCoO_2 which is based on the spin-state quasidegeneracy of CoO_6 octahedral complex in oxides and the specific lattice geometry of the CoO_2 planes in layered cobaltates. The model naturally explains the strong correlations found in the sodium-rich region due to the spin-polaron formation. We derived effective interactions in a Fermi-liquid regime and discussed their impact on spin fluctuations. The model predicts superconductivity mediated by the spin-state fluctuations of Co^{3+} ions, at experimentally observed compositions. The basic idea behind the model is that due to the 90° d - p - d pathway in the edge-shared structure, the electron transport in Na_xCoO_2 is entangled with low-lying $S = 1$ magnetic states of Co^{3+} ions which become an essential part of the Na_xCoO_2 physics. Given the simplicity and experimentally motivated design of the model, its success can hardly be accidental. Therefore, $t - \tilde{t}$ Hamiltonian can be regarded as a basic minimal model for Na_xCoO_2 . It may also have broader applications, *e.g.*, in oxides of Rh and Ir ions with a similar spin-orbital structure and lattice geometry.

ACKNOWLEDGMENTS

We would like to thank B. Keimer, J. Sirker, and M.Z. Hasan for stimulating discussions. This work was partially supported by the Ministry of Education of Czech Republic (MSM0021622410).

¹ K. Takada, H. Sakurai, E. Takayama-Muromachi, F. Izumi, R.A. Dilanian, and T. Sasaki, *Nature (London)* **422**, 53 (2003).

² N.P. Ong and R.J. Cava, *Science* **305**, 52 (2004).

³ Y. Wang, N.S. Rogado, R.J. Cava, and N.P. Ong, *Nature (London)* **423**, 425 (2003).

⁴ M.L. Foo, Y. Wang, S. Watauchi, H.W. Zandbergen, T. He, R.J. Cava, and N.P. Ong, *Phys. Rev. Lett.* **92**, 247001 (2004).

⁵ C. Bernhard, A.V. Boris, N.N. Kovaleva, G. Khaliullin, A.V. Pimenov, Li Yu, D.P. Chen, C.T. Lin, and B. Keimer, *Phys. Rev. Lett.* **93**, 167003 (2004).

⁶ S.P. Bayrakci, I. Mirebeau, P. Bourges, Y. Sidis, M. En-

derle, J. Mesot, D.P. Chen, C.T. Lin, and B. Keimer, *Phys. Rev. Lett* **94**, 157205 (2005).

⁷ G. Gašparović, R.A. Ott, J.-H. Cho, F.C. Chou, Y. Chu, J.W. Lynn, and Y.S. Lee, *Phys. Rev. Lett* **96**, 046403 (2006).

⁸ C. Bernhard, Ch. Niedermayer, A. Drew, G. Khaliullin, S. Bayrakci, J. Stremper, R.K. Kremer, D.P. Chen, C.T. Lin, and B. Keimer, *Europhys. Lett.* **80**, 27005 (2007).

⁹ D. Qian, L. Wray, D. Hsieh, D. Wu, J.L. Luo, N.L. Wang, A. Kuprin, A. Fedorov, R.J. Cava, L. Viciu, and M.Z. Hasan, *Phys. Rev. Lett.* **96**, 046407 (2006).

¹⁰ T. Shimojima, K. Ishizaka, S. Tsuda, T. Kiss, T. Yokoya,

- A. Chainani, S. Shin, P. Badica, K. Yamada, and K. Togano, *Phys. Rev. Lett.* **97**, 267003 (2006).
- ¹¹ D. Qian, L. Wray, D. Hsieh, L. Viciu, R.J. Cava, J.L. Luo, D. Wu, N.L. Wang, and M.Z. Hasan, *Phys. Rev. Lett.* **97**, 186405 (2006).
- ¹² T. Valla, P.D. Johnson, Z. Yusof, B. Wells, Q. Li, S.M. Loureiro, R.J. Cava, M. Mikami, Y. Mori, M. Yoshimura, and T. Sasaki, *Nature* **417**, 627 (2002).
- ¹³ V. Brouet, A. Nicolaou, M. Zacchigna, A. Tejada, L. Patthey, S. Hébert, W. Kobayashi, H. Muguerra, and D. Grebille, *Phys. Rev. B* **76**, 100403(R) (2007).
- ¹⁴ R.E. Schaak, T. Klimczuk, M.L. Foo, and R.J. Cava, *Nature (London)* **424**, 527 (2003).
- ¹⁵ P.W. Anderson, *Science* **235**, 1196 (1987).
- ¹⁶ K. Takada, K. Fukuda, M. Osada, I. Nakai, F. Izumi, R.A. Dilanian, K. Kato, M. Takata, H. Sakurai, E. Takayama-Muromachid, and T. Sasaki, *J. Mater. Chem.* **14**, 1448 (2004).
- ¹⁷ C.J. Milne, D.N. Argyriou, A. Chemseddine, N. Aliouane, J. Veira, S. Landsgesell, and D. Alber, *Phys. Rev. Lett.* **93**, 247007 (2004).
- ¹⁸ M. Karppinen, I. Asako, T. Motohashi, and H. Yamauchi, *Chem. Mater.* **16**, 1693 (2004).
- ¹⁹ See, *e.g.*, Q.-H. Wang, D.-H. Lee, and P.A. Lee, *Phys. Rev. B* **69**, 092504 (2004).
- ²⁰ $t_{2g}^4 e_g^2 S = 2$ configuration is not accessible by hopping.
- ²¹ S. Maekawa, T. Tohyama, S.E. Barnes, S. Ishihara, W. Koshibae, and G. Khaliullin, *Physics of Transition Metal Oxides*, Springer Series in Solid State Sciences, vol.144 (Springer-Verlag, Berlin, 2004).
- ²² M.W. Haverkort, Z. Hu, J.C. Cezar, T. Burnus, H. Hartmann, M. Reuther, C. Zobel, T. Lorenz, A. Tanaka, N.B. Brookes, H.H. Hsieh, H.-J. Lin, C.T. Chen, and L.H. Tjeng, *Phys. Rev. Lett.* **97**, 176405 (2006).
- ²³ S. Yamaguchi, Y. Okimoto, H. Taniguchi, and Y. Tokura, *Phys. Rev. B* **53**, R2926 (1996).
- ²⁴ R. Caciuffo, D. Rinaldi, G. Barucca, J. Mira, J. Rivas, M.A. Seïnarís-Rodríguez, P.G. Radaelli, D. Fiorani, and J.B. Goodenough, *Phys. Rev. B* **59**, 1068 (1999).
- ²⁵ S. Zhou, M. Gao, H. Ding, P.A. Lee, and Z. Wang, *Phys. Rev. Lett.* **94**, 206401 (2005).
- ²⁶ J. Chaloupka and G. Khaliullin, (unpublished).
- ²⁷ W. Koshibae and S. Maekawa, *Phys. Rev. Lett.* **91**, 257003 (2003).
- ²⁸ G. Lang, J. Bobroff, H. Alloul, P. Mendels, N. Blanchard, and G. Collin, *Phys. Rev. B* **72**, 094404 (2005).
- ²⁹ G. Khaliullin, *Prog. Theor. Phys. Suppl.* **160**, 155 (2005).
- ³⁰ M. Roger, D.J.P. Morris, D.A. Tennant, M.J. Gutmann, J.P. Goff, J.-U. Hoffmann, R. Feyerherm, E. Dudzik, D. Prabhakaran, A.T. Boothroyd, N. Shannon, B. Lake, and P.P. Deen, *Nature (London)* **445**, 631 (2007).
- ³¹ C.A. Marianetti and G. Kotliar, *Phys. Rev. Lett.* **98**, 176405 (2007).
- ³² M. Daghofer, P. Horsch, and G. Khaliullin, *Phys. Rev. Lett.* **96**, 216404 (2006).
- ³³ J. Bobroff, G. Lang, H. Alloul, N. Blanchard, and G. Collin, *Phys. Rev. Lett.* **96**, 107201 (2006).
- ³⁴ M.D. Johannes and D.J. Singh, *Phys. Rev. B* **70**, 014507 (2004).